Electrochemical Bond-Breaking Reactions: A Comparison of Large Scale Simulation Results with Analytical Theory

August Calhoun,[†] Marc T. M. Koper,[‡] and Gregory A. Voth*[,†]

Department of Chemistry and Henry Eyring Center for Theoretical Chemistry, University of Utah, Salt Lake City, Utah 84112, and Schuit Institute of Catalysis, Laboratory of Inorganic Chemistry and Catalysis, Eindhoven University of Technology, 5600 MB Eindhoven, The Netherlands

Received: December 9, 1998; In Final Form: February 17, 1999

The adiabatic free energy surface for the electrochemically induced dissociation of a methyl halide MeX ($MeX + e^- \rightarrow Me + X^-$) is computed from molecular dynamics (MD) simulations based on an underlying Hamiltonian developed to describe such processes. A two-dimensional free energy surface as a function of a collective solvent coordinate and the intramolecular Me−X bond length is computed. The theoretical basis of the simulations is a novel extension of the Anderson−Newns Hamiltonian to describe the coupling of the electron transfer to the bond-breaking process. A comparison of the simulation results is made with the standard analytical theory which is developed by virtue of several simplifying assumptions. It is found that the nonlinear microscopic features of the system produce significant deviations from the predictions of the analytical model.

I. Introduction

The electrochemical interface is of fundamental importance in a number of chemical processes. For example, the unique features of the interface can provide catalytic properties which are important in chemical synthesis. Among other things, an understanding of the way in which interfacial electron transfer promotes chemical reactions in the electrochemical context is crucial for our ability to control and modify these catalytic properties. The goal of the present investigation is therefore to explore an electrochemically induced reaction at a microscopic level through large scale computer simulations, and then to compare the results of the simulation with the predictions of a simplified analytical model.

Electrochemical reduction of organic molecules may result in a dissociation step where two molecular fragments break apart (i.e., $R-X + e^- \rightarrow R + X^-$). This process implies a very short lifetime intermediate with an excess negative charge. Experimentally, it has been observed that alkyl halides in a polar solvent do undergo this sort of bond-breaking reaction upon electron transfer (ET) from an electrode.[1] The alkyl halide negative intermediate which is formed upon the electron transfer is a rather short-lived species which rapidly dissociates. Some phenomenological theoretical work on this subject has shown that a concerted mechanism is a reasonable description of the electrochemical bond-breaking reaction.[1−4] These models, combined with ab initio calculations, have roughly predicted the proper solvent activation barrier for the bond-breaking ET (BBET) reaction in water. They have also recently been extended to treat cage and entropy effects.[5]

Recently, Koper and Voth[6] have developed a more complete Hamiltonian-based analytical approach for BBET reactions which recovers the results of refs 1−4 in certain limits. The key term in the Koper−Voth Hamiltonian effectively acts as a switching function between the bonded and unbonded states of the redox species as the ET reaction with the electrode occurs. Since this is a Hamiltonian approach, it can also be incorporated within a molecular dynamics (MD) simulation framework. Thus, a realistic solvent and electrode model can be used to estimate the free energy of electrochemical BBET at the microscopic level.

The application of our resulting simulation methodology is nominally to the electrochemical dissociation of CH_3Cl ($CH_3Cl + e^- \rightarrow CH_3 + Cl^-$) in water at a noble metal electrode (Pt). The uncertainties in certain parameters such as the condensed phase value of the methyl chloride electron acceptor level (LUMO) qualifies any claim that we are studying the actual CH_3Cl BBET reaction (this is a goal for the future). However, the primary focus of this work is to compare the results of the explicit simulations with those from analytical theory in order to judge the validity of the latter. This comparison is unaffected by uncertainties in the various parameters.

The present paper is organized as follows: In section II the basic MD model and methodology is described. Then, in section III the results are reported, while concluding remarks are given in section IV.

II. Model and Methods

The Hamiltonian in the simulation model is closely related to that of Koper and Voth[6] and consists of three parts,

$$H = H_{\text{solvent}} + H_{\text{elect}} + H_{\text{bb}} \tag{1}$$

where H_{solvent} is the part of the Hamiltonian which describes the solvent and solvent−electrode interactions, H_{elect} is the net electronic contribution due to the transferring electron, and H_{bb} is an additional term that couples the electronic population of the redox orbital on the molecule to the bond within the redox species.[6] The various terms will be described in detail below.

A. The Electronic Hamiltonian. The Anderson−Newns Hamiltonian[7−10] is used as the basis for the term H_{elect} in eq 1, which describes a single orbital on a redox species in solution coupled to the continuum of metal electrode states. This

* Corresponding author.
† University of Utah.
‡ Eindhoven University of Technology.

10.1021/jp984696i CCC: $18.00
Published on Web 04/10/1999

approach was first developed by Schmickler,[9] and it, or extended forms of it, has been applied both analytically and computationally to a number of electrochemical systems.[11−18] This part of the Hamiltonian can be written in second quantized form as

$$H_{\text{elect}} = (\epsilon_a + \Delta E)n_a + \sum_k (\epsilon_k n_k + V_{ak}c_k^\dagger c_k + V_{ka}c_k^\dagger c_a) \quad (2)$$

where ϵ_a is the vacuum energy level of the redox species electronic orbital $|a\rangle$ which is involved in the ET with the electrode and ΔE is the instantaneous energy shift of this orbital energy due to its interaction with the fluctuating electrochemical environment (i.e., it is the collective "solvent" coordinate).[16] The redox orbital has associated with it an occupation number operator n_a, which is equal to either 0 or 1, depending on its occupancy. The k's in eq 2 index the metal electronic states, and the V_{ak} terms represent the metal−redox orbital couplings.

Within the Born−Oppenheimer approximation, it is possible to find an analytical expression for the electronic energy of the system, E_0, as a function of ΔE, the collective solvent coordinate, i.e.,

$$E_0(\Delta E) = \frac{\Delta E}{2} + \frac{1}{\pi}(\epsilon_a - \Delta E - \epsilon_F)\tan^{-1}\left(\frac{\epsilon_F - \epsilon_a + \Delta E}{\Delta}\right) + \frac{\Delta}{2\pi}\ln\left[(\epsilon_a - \Delta E - \epsilon_F)^2 + \Delta^2\right] \quad (3)$$

The above expression can be readily incorporated into an MD simulation because it is a function of the nuclear positions of the system only (i.e., the solvent coordinate).[15−17] The experimental value of ϵ_a, or some other estimate, can be used, and the electronic coupling, Δ, can be computed from ab initio methods or estimated as well.[19,20] The Fermi level, ϵ_F, is an experimentally adjustable parameter which can be related to the electrode overpotential. Also, the average electronic population (the quantum mechanical expectation value), $\langle n_a(\Delta E)\rangle$, can be written as[9,11]

$$\langle n_a(\Delta E)\rangle = \frac{1}{2} + \frac{1}{\pi}\tan^{-1}\left(\frac{\epsilon_F - \epsilon_a + \Delta E}{\Delta}\right) \quad (4)$$

This continuous function of the collective solvent coordinate is in essence the electronic reaction coordinate which can be used to compute the average population of the redox orbital at any point in the MD simulation.

On the basis of the above analysis, the electronic energy and average population is seen to be a unique function of the collective solvent coordinate, which is given by[16]

$$\Delta E = -(V_{\text{solvent−ion}} - V_{\text{solvent−ion image}}) \quad (5)$$

This function is defined in the traditional Marcus picture as[16]

$$\Delta E = -\left(\sum_i^N \frac{q_i e}{r_{i,\text{ion}}} - \sum_j^N \frac{q_j e}{r_{j,\text{image}}}\right) \quad (6)$$

which is the sum of all of the solvent partial charge (q_i) interactions with a unit electronic charge at the redox site (e) and the redox image (reflected through the metal surface in the perfect conductor approximation for the metal ($-e$)).[16,17] This term can also be thought of as a difference potential, where the only change between the two electronic states is the ionic charge. Thus, *without* the bond breaking aspects of the problem, MD simulations of the ET reaction with the electrode can be performed with the Hamiltonian[15−17]

$$H_0 = H_{\text{solvent}} + E_0(\Delta E) \quad (7)$$

The bond-breaking term is critical, however, and this is now described.

B. Bond-Breaking Terms in the Hamiltonian. An additional bond-breaking term was proposed by Koper and Voth[6] to extend the Anderson−Newns formalism to describe electrochemical bond-breaking processes. If the ET is coupled to the molecular bonding state of the redox species, e.g., the redox orbital is an antibonding orbital, then an ET event with an electrode can be followed by a molecular dissociation (see, e.g., Figure 1). Experimental and theoretical investigations have shown that this is indeed the case, and that the BBET proceeds in a concerted single step manner.[1] Thus, a natural second quantized operator may be constructed from the redox orbital population operator n_a. This operation is given by[6]

$$H_{\text{bb}} = (1 - n_a)V_{\text{bonding}} + n_a V_{\text{antibonding}} \quad (8)$$

The first term in this equation switches off a bond (V_{bonding}) in a redox species as an antibonding orbital is populated (by electrochemical ET). Another function, in this case an antibonding function ($V_{\text{antibonding}}$), is switched on by the second term as the antibonding orbital is occupied.

The H_{bb} term in the present simulation model is given by a slightly modified version of eq 8, i.e.,

$$H_{\text{bb}} + (1 - n_a)[V_{\text{Morse}} + V_{\text{solvent}}] + n_a[V_{\text{rep}}] \quad (9)$$

where the V_{Morse} and V_{rep} are Koper and Voth's terms V_{bonding} and $V_{\text{antibonding}}$, respectively.[6] (The parameters for the Morse functions are taken from ref 4.) The additional term V_{solvent} is the reactant methyl chloride−solvent Coulombic interaction. It should be noted that the Koper−Voth analytical model of ref 6 does not contain the latter term (i.e., it is assumed that the reactant is nonpolar). It is not straightforward to incorporate the dipolar solvation into the analytic model, but it can be done approximately by modeling the reactant solvation through a linear response model and then neglecting the remaining dependence of the redox orbital population, $\langle n_a\rangle$, on the term V_{solvent}. The free energy contribution from this neglected term is significantly smaller than the electrostatic interaction with the charged CH_3Cl^- metastable species.

The particular treatment of the term H_{bb} in the present work is certainly a specific case for a more general formalism where a switching function like eq 8 can be utilized to couple two generic physical states of the redox species with the electrochemical ET. For example, a donated electron from the electrode electron could modify the electronic structure of an adsorbed molecular redox species without leading to a bond-breaking process, and thus it is possible to incorporate this effect into a simulation framework with a term like eq 8. In general, two electronic states of the redox species, $|1\rangle$ and $|2\rangle$, may therefore be coupled to the electrochemical ET process by a term

$$H_{12} = (1 - n_a)V_1 + n_a V_2 \quad (10)$$

which would replace the term H_{bb} in eq 1. For example, these states could be two bonded states with different electronic potential energy surfaces which result in different vibrational and structural characteristics. Also, the redox species−solvent interactions could be coupled to the ET process consistently via this formalism. This natural generalization beyond the original bond-breaking formalism of Koper and Voth therefore

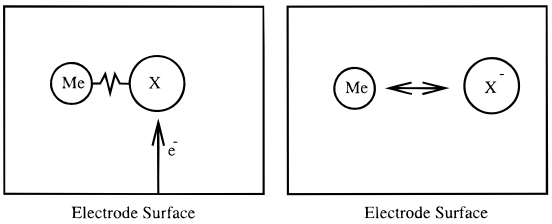

Figure 1. A schematic diagram of the BBET process. This shows the electron being transferred to the CH_3X redox species followed by a dissociation of the radical. The reaction is thought to proceed in a concerted manner.

opens up the study of a large number of electrochemically related processes through computer simulation.

C. Simulation Models. The specific system in the present study is a model for a CH_3Cl molecule near a Pt(111) electrode surface in water. Therefore, the chemical reaction modeled here is $CH_3Cl + e^- \rightarrow CH_3 + Cl^-$. A redox orbital on the chlorine atom was coupled to the metal electronic states with the Hamiltonian in eq 1, and the population of the redox orbital was coupled to the CH_3Cl intramolecular bond with the bond-breaking part of the total Hamiltonian. The CH_3Cl molecule was modeled as a two-site diatomic molecule, so the methyl fragment was treated in the united atom approximation. The TIPS parameters[22,23] for liquid CH_3Cl were used to describe the water-CH_3Cl interactions in the MD simulation (i.e., Coulomb plus Lennard−Jones site−site interactions).

A total of 320 SPC/F_2 water molecules[24] were included in the molecular dynamics cell, which had dimensions of 24.93 Å × 19.16 Å × 42.33 Å ($x-y-z$). The water molecules were restricted to be in the top half of the molecular dynamics cell by the metal surface, and the image of the CH_3Cl and of the electronic population on the redox site were reflected through the metal surface in the perfect conductor approximation for the electrode.[17] The solvent, therefore, interacts with the CH_3-Cl and the CH_3Cl image, both of which have a variable charge due to the ET process with the electrode. The images of the water molecules were not included in the present model because this effect is modeled in a static way through the water−metal interaction.[25,26] The entire molecular dynamics cell was replicated in three dimensions via the Ewald summation, which, including the ion image, results in a charge neutral cell.[27] Periodic boundary conditions were used, and the box size in the z direction was adjusted to yield the bulk density of water in the center of the water portion of the cell. The x and y dimensions were chosen to be commensurate with an integer number of Pt(111) unit cells.[15,25,26,28] The equations of motion were integrated with a multiple time step algorithm based on the velocity Verlet method,[29,30,31] and a Nose−Hoover chain of length 2 was attached to each particle for temperature control and ergodic sampling.[32,33] A small time step of $^1/_4$ fs was used to integrate the intramolecular modes while a large time step of 1 fs was used to integrate the intermolecular modes in the equations of motion. The average distance of the CH_3Cl molecule and product fragments from the Pt electrode surface was found to be 7.5 Å. The electronic coupling was chosen to be 55 meV because this value is in a reasonable range for a typical ET reaction. Also, this is in accord with ab initio estimates.[19,20] The vacuum ET acceptor energy level of the MeCl molecule was taken to be that of Cl (−3.617 eV), and the Fermi level of the electrode was chosen to be 7.98 eV so as to yield a zero overpotential in the analytical model of ref 6.

The detailed composition of the H_{bb} term in the present model is given by

TABLE 1: Parameters Utilized in the BBET Part of the Hamiltonian

D_e (kcal/mol)	r_0 (Å)	ω (cm^{-1})	μ (g/mol)
83	1.78	732	10.54

$$H_{bb} + (1 - n_a)[V_{Morse} + V^{Coulomb}_{CH_3,solvent} + V^{Coulomb}_{Cl,solvent} - V^{Coulomb}_{Cl_3,Cl}(Ewald)] + n_a[V_{rep}] \quad (11)$$

where the V_{Morse} and V_{rep} are similar to Koper and Voth's terms.[6] The Morse bonding term has the usual form

$$V_{Morse} = D_e(1 - e^{-a(r-r_0)})^2 \quad (12)$$

where D_e is the gas phase dissociation energy

$$a = \omega[\mu/2D_e]^{1/2} \quad (13)$$

and ω is the vibrational frequency around the minimum r_0. The repulsive antibonding term in eq 11 has the form

$$V_{rep} = D_e\, e^{-2a(r-r_0)} \quad (14)$$

The numerical values of the parameters for V_{Morse} and V_{rep} are given in Table 1. The terms $V^{Coulomb}_{CH_3,solvent}$ and $V^{Coulomb}_{Cl,solvent}$ in eq 11 are the methyl chloride−solvent Coulombic interactions, while $V^{Coulomb}_{Cl,solvent}$(Ewald) is the intramolecular Coulombic interaction resulting from the Ewald potential which must be removed. The expression in eq 11 assumes that the ion−water and methyl−water Lennard-Jones terms are the same in both electronic states, which should be a reasonable approximation. The partial charge on the CH_3 and Cl sites gets switched off as the electron is transferred to the Cl atom from the electrode.

Two coordinates (the collective solvent coordinate ΔE and the methyl chloride bond length r) define the free energy surface for BBET,[6] which can be computed via MD simulation. The free energy can be written as a configurational average

$$F(\Delta e, r) = -k_B T \ln[\int d\mathbf{p}\, d\mathbf{q}\, \delta[\Delta e - \Delta E(\mathbf{q})]\, \delta[r - r'(\mathbf{q})] e^{-\beta H(\mathbf{q})}] \quad (15)$$

where Δe is a particular value of the collective reaction coordinate, r is a particular value of the methyl chloride bond length r', and $\boldsymbol{q}$ is a multidimensional vector composed of all the system coordinates. The Hamiltonian H in eq 15 is the adiabatic electronic ground-state solution for eq 1.

A two-dimensional umbrella sampling technique was utilized to sample the free energy surface by virtue of a harmonic umbrella potential of the form

$$V^i_{umbrella}(\Delta E, r) = \frac{k_{\Delta E}}{2}(\Delta E - \Delta e_i)^2 + \frac{k_r}{2}(r - r_i)^2 \quad (16)$$

where i is the window index.

A two-dimensional version of the weighted histogram analysis (WHAM) of Kumar et al.[34,35] was also implemented to match the umbrella windows together. This method is essentially a global least-squares fit to the simulation data which takes a weighted average over the statistics from each separate simulation into account when computing the probability of each bin. The WHAM procedure amounts to solving the following set of equations self-consistently

$$\langle P(\Delta e,r)\rangle = \sum_i^M \frac{n_i\langle \rho_i(\Delta e,r)\rangle_i}{\sum_j^M n_j \exp(-\beta(V^j_{\text{umbrella}}(\Delta e,r) - F_j))} \quad (17)$$

$$F_i = -(1/\beta)\ln[\int \mathrm{d}(\Delta e)\int \mathrm{d}r\,\langle P(\Delta e,r)\rangle \times \exp(-\beta(V^j_{\text{umbrella}}(\Delta e,r)))] \quad (18)$$

to find the values of the f_i, which are the optimal additive constants used to adjust the umbrella windows. The unbiased distribution is P, the biased distributions from the individual umbrella sampling windows are ρ_i, and the number of samples in each window is n_i.

The free energy surface may also be estimated analytically if a linear response model for the solvent is employed. A linear response model for the solvent fluctuations is a useful tool for understanding the qualitative features of the free energy surface.[11,21] The free energy of fluctuations in this solvent model can be written as

$$F_{\text{solvent}} = F_{\text{MeCl,min}} + \frac{1}{4\lambda}(\Delta e - \Delta e_0)^2 \quad (19)$$

where λ is the solvent reorganization free energy, Δe_0 is the minimum of the solvent free energy coordinate in the reactant state, and $F_{\text{MeCl,min}}$ is the solvation free energy corresponding to that minimum. These parameters were computed from MD simulations of the diabatic CH_3Cl (undissociated) reactant state. In essence, the accuracy of the linear response approximation in eq 19 is the key thing which is under examination in this paper through our computer approach and its explicit treatment of the microscopic solvent−solute and solvent−solvent interactions.

III. Results

The free energy surface computed from the MD simulations with the BBET Hamiltonian is shown in the top panel of Figure 2. This free energy surface is a result of 2700 umbrella sampling calculations. Each umbrella "window" consisted of a 7 ps equilibration period, and a 20 ps data collection period. The parts of the free energy with the most error are near the edges of the surface. The important part of the surface, the barrier and well regions, were sampled the most. The statistical errors here are approximately 1 kcal/mol (computed from the standard deviation for different averaging intervals of the free energy calculation). The free energy surface shown in the upper part of Figure 2 represents 114 000 node hours of computation on parallel computers. This is equivalent to running a single present day high-end workstation for 13 years.

Several qualitative features of the free energy surface are readily apparent. First, there is a bound well where the CH_3Cl is stable and the electron has not been transferred from the electrode to the CH_3Cl. There is also an exit channel, because the CH_3Cl^- radical after ET is not stable and dissociates. Thus, the free energy surface clearly contains the essential characteristics of the BBET process: a stable CH_3Cl species, and an unstable CH_3Cl^- radical. Interestingly, there is a well in the exit channel where the methyl fragment and the chloride fragment are still in contact. This well, which is 7 kcal/mol below the barrier top in the exit channel, is a result of the explicit molecular nature of the solvent in the MD model. When the fragments are in contact, or separated by a single water molecule, the result is configurations with a lower free energy than when the fragments begin to separate, but are not separated enough to allow a water molecule between the fragments. There is an energy "cost" associated with making this hole in the solvent (the intermediate state); therefore, the contact fragment pair and solvent-separated fragment pair have a free energy barrier between them.

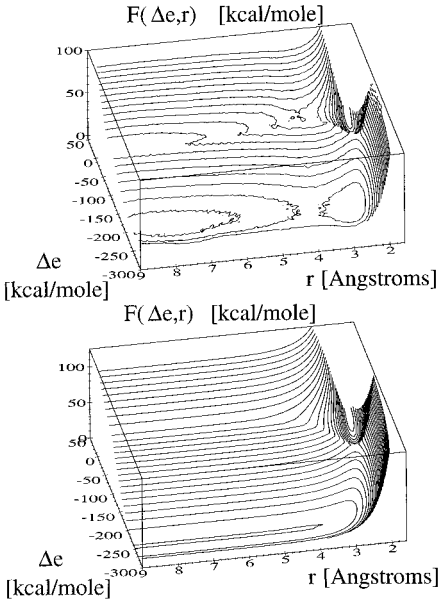

Figure 2. Surface plots of the adiabatic BBET free energy surface as computed from MD simulation (upper panel), and the linear response solvent model (lower panel). The reactant well and exit channel are clearly visible in both plots. The well corresponds to the neutral CH_3-Cl molecule, and the exit channel to the unstable charged radical.

TABLE 2: Free Energy Barriers for the $CH_3Cl + e^- \rightarrow CH_3 + Cl^-$ BBET Reaction Computed from MD Simulation and Analytic Theory[a]

method	forward barrier (kcal/mol)	overpotential (η) (kcal/mol)
simulation	37 ± 1	10
analytic theory	37	0
analytic theory	42	10

[a] Theory of refs 1 and 6, the latter being in the small electronic coupling limit (eq 20).

The dominant barrier for the BBET reaction is, however, significantly higher than the additional barrier in the dissociation channel. From the reactant well to the metastable CH_3Cl^- well, the MD simulation data reveals the barrier to be 37 kcal/mol (cf. Table 2).

The free energy surface for the BBET Hamiltonian computed with the analytical linear response solvent model based upon ref 6 is also shown in the lower panel of Figure 2. The reorganization energy, λ, and the minimum of the neutral state free energy well, Δe_0, were determined from a single 50 ps MD simulation of the reactant CH_3Cl state with no umbrella potential. This trajectory sampled the free energy curve near the minimum, and a local harmonic fit was used to determine λ and Δe_0. The gross qualitative features of the surface computed with the linear response model for the solvent are similar to the accurate surface computed via simulation. Again, there is a bound well where the CH_3Cl is stable and the electron has not been transferred from the electrode to the CH_3Cl, and there is also an exit channel, because the CH_3Cl^- radical is not stable. There are, however, important qualitative differences revealed upon closer inspection. One notable feature is that the exit

channel is rather featureless with only a steep repulsive wall. This contrasts with the simulation results which show a free energy well in the exit channel. Another key qualitative difference is a positive free energy of reaction overpotential in the simulation data which is not present in the analytic model for the given set of parameters.

The plots in Figure 2 also reveal important *quantitative* differences between the simulation results and the analytical linear response model predictions. The curvature, minima, and reaction free energy (overpotential) differ considerably between the analytical model and the MD simulation data. This is due to the nonlinear response of the solvent in the MD simulation as the CH_3Cl bond is broken, which is in turn related to the change in the charge on the redox center from -0.25 in the CH_3Cl molecule to -1 for the chloride ion, and to the change in the volume exclusion effect from the Me fragment at different values for r. The primary quantitative difference between the simulation results and the analytical prediction is the previously mentioned 10 kcal/mol positive overpotential for the former in forming first the metastable $MeCl^-$ ion and then subsequently the Me and Cl^- fragments. The analytical model thus predicts a steady state concentration of the metastable ionic intermediate (and ultimately the products) which is too large by *7 orders of magnitude*. Interestingly, the *rate constant* for the ET event from the electrode to the MeCl is predicted to be roughly the same by both simulation and theory (cf. Table 2). However, the reaction *thermodynamics* are found to differ greatly.

It should be noted that the above comparison of the analytic model with the simulation results is based on the usage of a common electrode Fermi level in the underlying Hamiltonian (eq 1) which appears in both approaches. One might argue that a better approach is to compare the predictions of the analytical model with the results of simulation for a common overpotential, i.e., to adopt a more phenomenological picture which has its footing in experimentally specified quantities. Along these lines, the expression for the activation free energy ΔF_{act} in the analytical model is given to a good approximation by[1,6]

$$\Delta F_{act} = \frac{\lambda + D_e}{4}\left(1 + \frac{\eta}{\lambda + D_e}\right)^2 \qquad (20)$$

where η is the overpotential, λ is the reorganization free energy, and D_e is the gas phase dissociation energy of the MeCl bond. For the case of a 10 kcal/mol positive overpotential as observed in the simulation, the above expression predicts a kinetic barrier to ET of 42 kcal/mol, while the simulation barrier is found to be 37 kcal/mol as stated earlier (cf. Table 2). This difference in barrier corresponds to a difference of more than 3 orders of magnitude in the ET rate constant between the analytical prediction and the simulation result. The fundamental quantitative differences between the simulation results and the analytical predictions therefore do not disappear even when viewed by this alternative approach.

One-dimensional slices of the free energy surfaces reveal more interesting differences between the simulation results and the predictions of analytical theory. Near the saddle point at r_{CH_3Cl} is the transition state in the simulation data. A slice of the free energy surface along the solvent coordinate Δe at this value of r is shown in the top panel of Figure 3. Moving from the left to the right well at fixed r corresponds to the reaction $CH_3Cl + e^- \rightarrow CH_3 + Cl^-$. The curvature and minimum of the right well (CH_3Cl^- species) are different between the linear response solvent and MD simulation data. The differences in curvature in the two wells of the simulation data are reflected

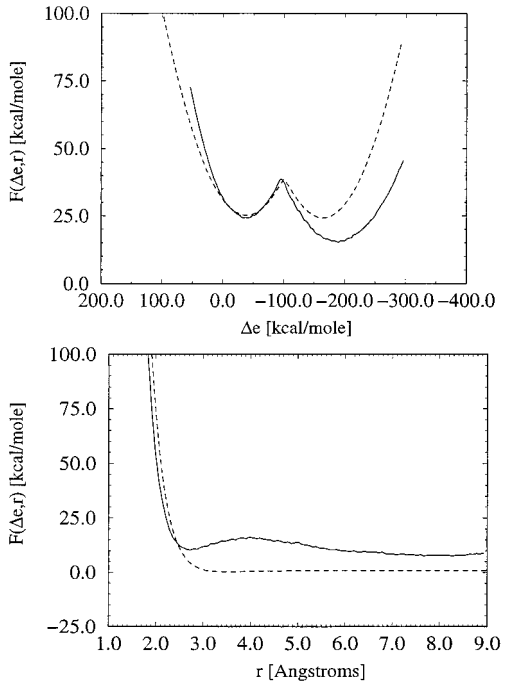

Figure 3. A slice from the free energy surface through the transition state at $r_{CH_3Cl} = 2.2$ Å (top panel). Note that the curvature is very different for the two wells in the simulation data (solid line), but the same for the linear response solvent model (dashed line). Slice from the free energy surface with $\Delta e = -225$ kcal/mol (bottom panel). This clearly shows the repulsive potential in the exit channel, with a well in the simulation data (solid line) where the fragments are still in contact.

in differences in the effective reorganization energy ($\lambda = 50$ in the left well versus $\lambda = 92$ for the right well). This is due to the nonlinear response of the solvent in the MD simulation as the CH_3Cl bond is broken. In contrast, the reorganization energy is the same in the two wells of the linear response model by definition. The nonlinear response of the solvent fluctuations is sensitive to the change in the charge on the redox center from -0.25 in the CH_3Cl molecule to -1 for the chloride ion. The solvent fluctuations are also coupled to the volume exclusion effect from the CH_3 fragment at different values for r.

A slice of the free energy surface along bond dissociation coordinate r for $\Delta e = -225$ kcal/mol is shown in the lower panel of Figure 3 (i.e., the exit channel). The well in the simulation results can clearly be seen here which is due to explicit microscopic solvation effects. The height of the barrier to leave the exit channel once an electron transfer has occurred is 7 kcal/mol, as stated earlier. This is not a small barrier, but it will not be the rate-limiting step for the BBET reaction because the height of the (primarily) solvent barrier is 37 kcal/mol from the MD simulation data. This fact was confirmed by studying MD trajectories initiated near the barrier top which always lead to the fragments dissociating.

As stated in an earlier paragraph, it is found that the effective reorganization energy, λ, depends on the state of the system, which is different for the molecular and the fragment states, as well as on the bond length or interfragment distance r. Furthermore, a λ determined from a local fit about a minimum often gives a poor fit of the entire free energy curve as obtained from the umbrella sampling procedure. Therefore, an alternative way of extracting the λ from the MD simulations is by subjecting the entire potential energy curve of one state to a parabolic fit, at least up to the transition state. The λ obtained in this way is close to another definition of the solvent reorganization energy, namely as the vertical energy shift from the diabatic state under

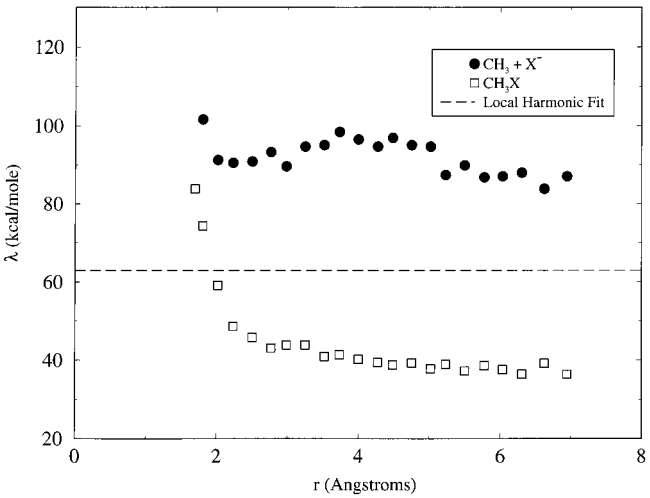

Figure 4. A plot of λ, the effective reorganization energy, as a function of r, the CH_3X intramolecular bond length (X = Cl). The reorganization energy is determined from global harmonic fits to the free energy surface at fixed values of r. The dashed line shows λ determined by a local harmonic fit to the reactant well (cf. eq 19).

consideration to the minimum of the other diabatic state (at equilibrium), as it effectively includes deviations from nonparabolicity of the overall diabatic energy curve. The solvent reorganization energies determined in this way, and their dependence of the bond length or interfragment distance r for both the molecule and the fragmented states, are shown in Figure 4. The λ determined from a global fit to the CH_3X (X = Cl) well is shown by the squares in Figure 4, and the λ determined from a global fit to the CH_3X^- well is shown by the filled circles. The λ as determined from a local fit about the CH_3X minimum (eq 19) is shown as the dashed line in Figure 4 and seen to give a poor description of the real solvent response. An interesting possibility is to improve the analytic model by adding a coordinate-dependent reorganization energy that has been fit to the simulation data, and this will be explored in the future.

The effects of the solvent structure in the exit channel can be introduced into the analytical model by including the fragment−fragment potential of mean force (PMF) into the $V_{\text{antibonding}}$ term of eq 8. The contour plot resulting from this procedure are shown in the lower panel of Figure 5 and compared to the exact simulation results shown in the upper panel. Certainly, this free energy surface looks more like that computed by simulation because it includes some microscopic solvent detail via the fragment PMF, but the agreement is still not quantitative, particularly with regards to the overpotential.

IV. Concluding Remarks

The free energy surface for a BBET reaction was computed through an explicit MD simulation and compared to the results based on an analytical linear response solvent model.[6] The latter model is found to not accurately reproduce all of the microscopic detail from the MD simulation results. Specifically, there is a significant free energy well for a contact fragment pair due to the microscopic features of the solvent and solute. In addition, the dependence of the reorganization free energy on the redox species charge state and dissociation coordinate is not accurately predicted by the linear response solvent model, nor is the reaction free energy (overpotential). The analytical model is thus seen to be a convenient tool for estimating trends and gross features, but it does not reproduce the quantitative details of the BBET free energy surface. While simple estimates for the free energy surface from the analytic model are very useful in

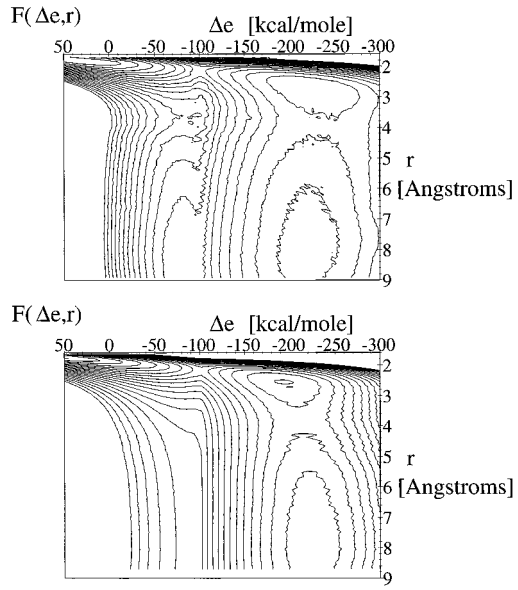

Figure 5. Contour plots of the adiabatic BBET free energy surface as computed from MD simulation (upper panel), and the linear response solvent model (lower panel) with the fragment PMF data added for the charged CH_3Cl^- state.

light of the computational cost of computing the surface via simulation, accurate results will require explicit computer simulations. Improvements to the analytic model will therefore be the subject of future research.

Acknowledgment. This research was supported by the Office of Naval Research and the Royal Netherlands Academy of Arts and Sciences (KNAW). Computations were carried out at the Aeronautical Systems Center Major Shared Resource Center at Wright-Patterson Air Force Base through a Department of Defense Grand Challenge Computing Grant, and at the National Center for Supercomputing Applications (NCSA) through NSF Metacenter grant no. MCA94P017P. We also gratefully acknowledge the University Utah Center for High Performance Computing for a generous grant of Silicon Graphics Origin 2000 time.

References and Notes

(1) Saveant, J. *Acc. Chem. Res.* **1993**, *455*, 26.
(2) Bertran, J.; Gallardo, I.; Moreno, M.; Saveant, J. *J. Am. Chem. Soc.* **1992**, *9576*, 114.
(3) Andrieux, C. P.; Gorande, A. L.; Saveant, J. *J. Am. Chem. Soc.* **1992**, *6892*, 114.
(4) Saveant, J. *J. Am. Chem. Soc.* **1987**, *6788*, 109.
(5) Andrieux, C. P.; Saveant, J.; Tardy, C. *J. Am. Chem. Soc.* **1998**, *4167*, 120.
(6) Koper, M. T. M.; Voth, G. A. *Chem. Phys. Lett.* **1998**, *100*, 282.
(7) Anderson, P. W. *Phys. Rev.* **1961**, *41*, 124.
(8) Newns, D. M. *Phys. Rev.* **1969**, *1123*, 178.
(9) Schmickler, W. *J. Electroanal. Chem.* **1986**, *31*, 204.
(10) Kornyshev, A.; Schmickler, W. *J. Electroanal. Chem* **1985**, *253*, 185.
(11) Sebastian, K. L. *J. Chem. Phys.* **1989**, *5056*, 90.
(12) Koper, M. T. M.; Schmickler, W. *Chem. Phys.* **1996**, *123*, 211.
(13) Koper, M. T. M. *J. Phys. Chem.* **1997**, *3168*, 101.
(14) Koper, M. T. M.; Mohr, J. H.; Schmickler, W. *Chem. Phys.* **1997**, *95*, 220.
(15) Straus, J. B.; Calhoun, A.; Voth, G. A. *J. Chem. Phys.* **1995**, *529*, 102.
(16) Calhoun, A.; Voth, G. A. *J. Phys. Chem.* **1996**, *10746*, 100.
(17) Calhoun, A.; Voth, G. A. *J. Electroanal. Chem.* **1998**, *450*, 253.
(18) Smith, B.; Hynes, J. T. *J. Chem. Phys.* **1993**, *6517*, 99.
(19) Ursenbach, C. P.; Voth, G. A. *J. Chem. Phys.* **1995**, *7569*, 103.
(20) Ursenbach, C. P.; Calhoun, A.; Voth, G. A. *J. Chem. Phys.* **1997**, *2811*, 106.

(21) Boroda, Y. G.; Calhoun, A.; Voth, G. A. *J. Chem. Phys.* **1997**, *8940*, 107.
(22) Jorgensen, W. L. *J. Am. Chem. Soc.* **1981**, *335*, 103.
(23) Jorgensen, W. L.; Chandrasekhar, J.; Madura, J. D.; Impey, R. W.; Klein, M. L. *J. Chem. Phys.* **1983**, *926*, 79.
(24) Lobaugh, J.; Voth, G. A. *J. Chem. Phys.* **1997**, *2400*, 106.
(25) Spohr, E.; Heinzinger, K. *Ber. Bunsen-Ges. Phys. Chem.* **1988**, *1358*, 92.
(26) Spohr, E.; Heinzinger, K. *Chem. Phys. Lett.* **1986**, *218*, 123.
(27) Perram, J. W.; Ratner, M. A. *J. Chem. Phys.* **1996**, *5274*, 104.
(28) Raghavan, K.; Foster, K.; Motakabbir, K.; Berkowitz, M. *J. Chem. Phys.* **1991**, *2110*, 94.
(29) Tuckerman, M.; Berne, B. J.; Martyna, G. J. *J. Chem. Phys.* **1992**, *1990*, 97.
(30) Humphreys, D. D.; Friesner, R. A.; Berne, B. J. *J. Phys. Chem.* **1994**, *6885*, 98.
(31) Stuart, S. J.; Zhou, R.; Berne, B. J. *J. Chem. Phys.* **1996**, *1426*, 105.
(32) Nosé, S. *J. Chem. Phys.* **1984**, *511*, 81.
(33) Martyna, G. J.; Klein, M. L.; Tuckerman, M. *J. Chem. Phys.* **1992**, *2695*, 97.
(34) Kumar, S.; Douzida, D.; Swendsen, R. H.; Kollman, P. A.; Rosenberg, J. M. *J. Comput. Chem.* **1992**, *1011*, 13.
(35) Roux, B. *Comput. Phys. Commun.* **1995**, *275*, 91.